Biochimica et Biophysica Acta 1818 (2012) 241–251

Contents lists available at ScienceDirect

Biochimica et Biophysica Acta

journal homepage: www.elsevier.com/locate/bbamem

Review

Molecular simulations and solid-state NMR investigate dynamical structure in rhodopsin activation ☆

Blake Mertz [a], Andrey V. Struts [a,b], Scott E. Feller [c], Michael F. Brown [a,d,*]

[a] Department of Chemistry and Biochemistry, University of Arizona, Tucson, AZ 85721, USA
[b] Department of Medical Physics, St. Petersburg State Medical University, St. Petersburg 194100, Russia
[c] Department of Chemistry, Wabash College, Crawfordsville, IN 47933, USA
[d] Department of Physics, University of Arizona, Tucson, AZ 85721, USA

ARTICLE INFO

Article history:
Received 26 June 2011
Received in revised form 1 August 2011
Accepted 1 August 2011
Available online 8 August 2011

Keywords:
G protein-coupled receptor
Membrane
Molecular dynamics
Solid-state NMR
Rhodopsin
Vision

ABSTRACT

Rhodopsin has served as the primary model for studying G protein-coupled receptors (GPCRs)—the largest group in the human genome, and consequently a primary target for pharmaceutical development. Understanding the functions and activation mechanisms of GPCRs has proven to be extraordinarily difficult, as they are part of a complex signaling cascade and reside within the cell membrane. Although X-ray crystallography has recently solved several GPCR structures that may resemble the activated conformation, the dynamics and mechanism of rhodopsin activation continue to remain elusive. Notably solid-state ^{2}H NMR spectroscopy provides key information pertinent to how local dynamics of the retinal ligand change during rhodopsin activation. When combined with molecular mechanics simulations of proteolipid membranes, a new paradigm for the rhodopsin activation process emerges. Experiment and simulation both suggest that retinal isomerization initiates the rhodopsin photocascade to yield not a single activated structure, but rather an ensemble of activated conformational states. This article is part of a Special Issue entitled: Membrane protein structure and function.

Contents

Abbreviations: CHARMM, Chemistry at Harvard Macromolecular Mechanics; EPR, electron paramagnetic resonance; FTIR, Fourier transform infrared; GPCR, G protein-coupled receptor; MD, molecular dynamics; Meta I, metarhodopsin I; Meta II, metarhodopsin II; 2MBD, 2-methyl-butadiene; 3MHT, 3-methyl-hexatriene; MM, molecular mechanics; POPC, 1-palmitoyl-2-oleoyl-*sn*-glycero-3-phosphocholine; PSB, protonated Schiff base; RDC, residual dipolar coupling; RQC, residual quadrupolar coupling; SDPC, 1-stearoyl-2-docosahexaenoyl-*sn*-glycero-3-phosphocholine; SDPE, 1-stearoyl-2-docosahexaenoyl-*sn*-glycero-3-phosphoethanolamine; QM, quantum mechanics

☆ This article is part of a Special Issue entitled: Membrane protein structure and function.

* Corresponding author at: Department of Chemistry and Biochemistry, University of Arizona, Tucson, AZ 85721, USA. Tel.: +1 520 621 2163; fax: +1 520 621 8407.
E-mail address: mfbrown@u.arizona.edu (M.F. Brown).

0005-2736/$ – see front matter © 2011 Published by Elsevier B.V.
doi:10.1016/j.bbamem.2011.08.003

1. Introduction

Rhodopsin is the G protein-coupled receptor (GPCR) responsible for dim light vision and plays a prominent role in our understanding of biological signaling. Investigating GPCRs lies at the forefront of pharmaceutical research, as they represent almost one-half of current drug targets [1]. In fact, rhodopsin is the most well-studied GPCR, on account of its relative ease of procurement and its well-characterized spectroscopic intermediates [2,3]. Upon photon absorption, an 11-*cis* → all-*trans* isomerization of the covalently bound inverse agonist retinal leads to initiation of the rhodopsin photocascade. This isomerization causes conformational changes within rhodopsin that allow interaction with the G protein transducin (G_t) in the cytosol. The signaling protein transducin acts as an intermediary between rhodopsin and its effector cGMP phosphodiesterase. Catalysis of GDP–GTP exchange by rhodopsin allows transducin to activate the cGMP phosphodiesterase, yielding hydrolysis of cGMP and closing of cyclic nucleotide-gated ion channels in the rod cellular plasma membrane. This last step leads to hyperpolarization of the rod and generation of a visual nerve impulse. Although the above signaling cascade is a blueprint for GPCR function, it remains incompletely understood at present—particularly for rhodopsin activation at the molecular level.

In this regard, structural biology has contributed insights into the workings of this system that are broadly significant for membrane function. The first GPCR crystal structure was of rhodopsin in the dark state [4]. Subsequent crystal structures of rhodopsin [5–10], opsin [11,12], the β_1- and β_2-adrenergic receptors [13–17], and the adenosine A_{2A} receptor [18] have now been solved, offering the potential for further mechanistic insight. Nonetheless, despite the availability of a number of GPCR structures, X-ray crystallography cannot completely explain membrane protein function. No structure has been solved in a native lipid bilayer environment. Additionally, each structure is a snapshot of the protein, and is unable to fully reveal the dynamics. Recently, our understanding of rhodopsin activation has been further advanced by reports of X-ray structures for the active Meta II state—yet, the results are complicated by opposite orientations for the retinal ligand obtained by different research groups [9,10]. Application of spectroscopic techniques such as nuclear magnetic resonance (NMR) are thus needed to provide structural data for trapped photointermediates in order to fill these essential gaps in knowledge of the activation process [19,20].

Below we summarize a solid-state ^{2}H NMR approach that is unique in that it can be used to investigate both structure and dynamics of retinal within the rhodopsin binding pocket [21]. The ^{2}H NMR method is mainly limited to the immediate vicinity of isotopic labels. However, computational simulations can add to the ^{2}H NMR data by examining the entire proteolipid system, thereby contributing to a more complete picture of the receptor activation process. Here we demonstrate how experiment and theory have a synergistic interplay that yields new insights into the activation mechanism of rhodopsin in a nativelike membrane environment. Solid-state NMR spectroscopy probes the changes in the local structure and dynamics of the retinal ligand of rhodopsin at a site-specific level. In addition, molecular dynamics simulations allow extension to longer time scales, thus enabling further investigation of the energy landscape of rhodopsin activation. Numerical simulations require accurate parameterization of the relevant molecular mechanics force fields, which has motivated us to carry out quantum mechanical calculations for retinal model compounds. Last, we show how the retinal methyl groups are implicated in rhodopsin activation, involving subsequent interaction with the signaling G protein transducin in visual excitation.

2. Rhodopsin: interface between experiment and simulation

Rhodopsin, the canonical GPCR, is composed of seven transmembrane helices connected by a series of extracellular and cytoplasmic loops [3]. Unlike most other GPCRs the activating ligand, retinal, is covalently bound to Lys^{296} on transmembrane helix 7 (H7). As noted above, upon absorption of a photon retinal undergoes an 11-*cis* → all-*trans* isomerization [2], initiating a photocascade culminating with activation of the G protein, transducin (Fig. 1). This photocascade consists of a spectroscopically well-defined series of intermediates: dark state → bathorhodopsin → lumirhodopsin → Meta I ⇄ Meta II [22]. It is important to appreciate that rhodopsin is unable to fully activate transducin until reaching the Meta II state. Because the equilibrium between the Meta I and Meta II states strongly depends on conditions such as pH, temperature, humidity, and membrane bilayer composition, one can physically trap these intermediates by

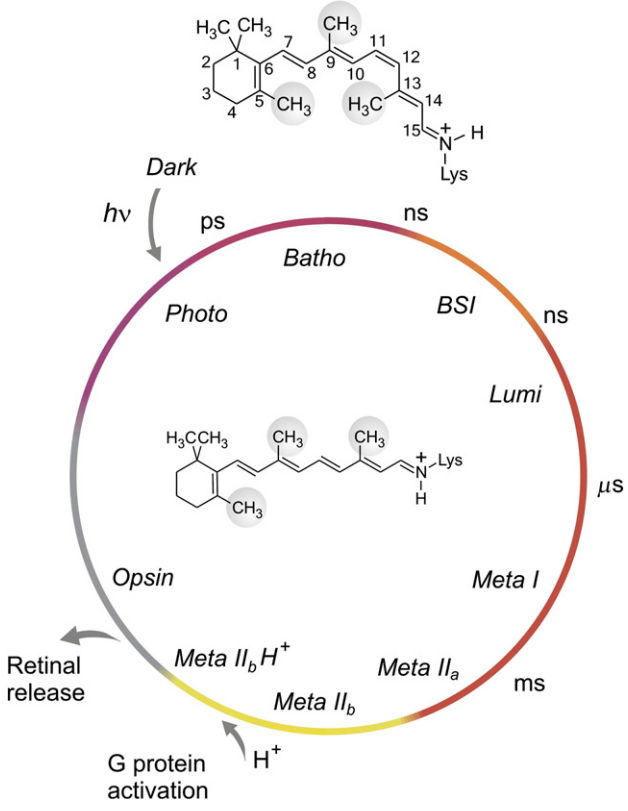

Fig. 1. Photocascade of rhodopsin underlies multiscale activation mechanism involving conformational changes with different time scales. Upon light absorption 11-*cis* to *trans* isomerization converts retinal from an inverse agonist to an agonist. Rhodopsin intermediates are designated as photorhodopsin, bathorhodopsin, blue-shifted intermediate (BSI), lumirhodopsin, metarhodopsin I, and metarhodopsin II. The Meta II state comprises an ensemble of Meta II$_a$, Meta II$_b$, and Meta II$_b$H$^+$ substates (activated ensemble mechanism). Note that various photoproducts can be trapped under different conditions of temperature, pH, or lipid composition.

changing thermodynamic state variables. This stabilization provides a means for studying the preactivated Meta I state as well as the fully activated Meta II state of rhodopsin. Techniques which have been used successfully in this regard include magnetic resonance methods, such as spin-label electron paramagnetic resonance (EPR) [23], solid-state ^{13}C NMR [20,24–30], and ^{2}H NMR spectroscopy [19,31–35].

2.1. Solid-state ^{2}H NMR line shapes are related to dynamical structure of retinal ligand

Solid-state ^{2}H NMR spectroscopy uses site-directed ^{2}H-labeling to investigate the local structure and dynamics of both proteins [19,32,33] and lipid bilayers [36–41]. In the case of membrane proteins, ^{2}H NMR provides orientational restraints (bond orientations), and when coupled with interatomic distance restraints it gives structural data analogous to solution NMR [19]. Residual quadrupolar couplings correspond directly to segmental order parameters, and can be measured along with dynamical parameters (nuclear spin relaxation rates). A more detailed explanation of this method can be found elsewhere [34]. In our research, retinal is synthesized with ^{2}H labels on a specific methyl group (C1-, C5-, C9-, or C13-methyl), reincorporated into the binding pocket of opsin, and recombined with synthetic phospholipids to produce a nativelike environment [19,32,33]. Isotopic labeling of each methyl group allows one to examine various regions of the binding pocket, and thus to delineate specific interactions during the activation of rhodopsin.

2.2. Molecular simulations further characterize structural dynamics and fluctuations of membrane proteins

An important aspect is that ^{2}H NMR line shape analysis can be used as a means for validating computational simulations, which in turn can extend and aid the interpretation of spectroscopic observables. A representative example of this approach to spectral line shape analysis can be found in Fig. 2. Experimental ^{2}H NMR spectra of the retinal methyl groups are related to bond orientations with respect to the membrane normal. The theoretical ^{2}H NMR spectra of aligned samples can be calculated using $C-C^{2}H_3$ bond orientational distributions (relative to the membrane) as obtained from molecular dynamics (MD) simulations, thus allowing testing of different molecular models [32,33,42]. Subsequently it is possible to directly compare the simulated spectra to the experimental spectra, providing an excellent means to use simulation in a complementary way with experimental observables.

3. Molecular dynamics calculations allow testing of specific counterion models for rhodopsin

One of the major shortcomings of the ^{2}H NMR approach as applied to the retinal cofactor [35] is that it does not provide structural details for the entire protein. However, MD simulations can be used in combination with ^{2}H NMR to provide knowledge of the dynamics of the entire proteolipid system. Since rhodopsin was the first published GPCR crystal structure, it has been the most extensively studied by computation. Namely, it has been used to examine various aspects of GPCR activation including overall structural changes [43,44], lipid effects [45,46], oligomerization [47,48], and lipid–protein interactions [49,50], among others.

Among the hotly debated aspects of the rhodopsin activation mechanism has been the deprotonation event of the protonated Schiff base (PSB) in the activated Meta II state (Fig. 2). In the originally proposed counterion-switch model [51], rhodopsin has a neutral binding pocket, where Glu^{113} is deprotonated and acts as a counterion to the PSB. The protonated Glu^{181} residue acts as a Brønsted acid and undergoes proton transfer to the conjugate base Glu^{113} upon isomerization of the retinal ligand, thus accommodating deprotonation of the Schiff base in the active Meta II state (Fig. 2a). Based on more recent data, an alternative complex-counterion model has also been developed [52],

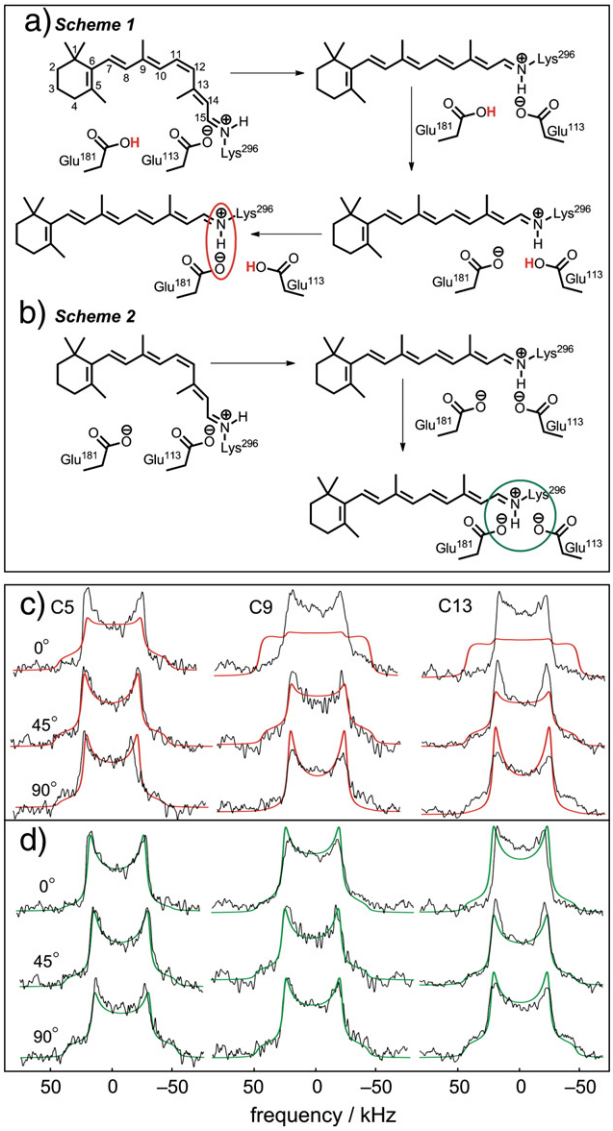

Fig. 2. Molecular dynamics (MD) simulations of rhodopsin allow testing of models for retinal Schiff base counterion based on bond angle distributions from solid-state ^{2}H NMR spectroscopy. (a) Scheme 1 shows a counterion-switch model where the counterion of the retinylidene protonated Schiff base (PSB) changes from Glu^{113} to Glu^{181} upon photoisomerization. (b) Scheme 2 is an alternative complex-counterion model in which both Glu^{113} and Glu^{181} are counterions to the retinal PSB of rhodopsin. (c, d) Results of MD simulations are compared to experimental ^{2}H NMR spectra for retinal ^{2}H-labeled at the C5-, C9-, or C13-methyl groups in the Meta I state at −100 °C in aligned membranes. The orientation of the average membrane normal to the magnetic field was $\theta = 0$, 45, and 90°. Theoretical ^{2}H NMR spectra (continuous lines) are shown compared to experimental results for (c) the counterion-switch model and (d) the complex-counterion model. Note the complex-counterion model agrees best with experimental solid-state ^{2}H NMR spectra.
Figure adapted with permission from Ref. [55].

assigning a negative charge to the binding pocket. Here both Glu^{113} and Glu^{181} are deprotonated, with Glu^{113} accepting the proton from the PSB (Fig. 2b). Several computational studies have examined this problem using different approaches, including Poisson–Boltzmann methods, classical MD simulations, and hybrid quantum mechanics/molecular mechanics (QM/MM) approaches [53,54], with results tending to support the complex-counterion mechanism.

To definitely answer this question, we set out to simulate both counterion models using long time-scale classical MD simulations, and then compared the results to experimental ^{2}H NMR data (Fig. 2). Each system consisted of a rhodopsin molecule embedded in a ternary lipid bilayer (1-stearoyl-2-docosahexaenoyl-*sn*-glycero-3-phosphocholine

(SDPC)/1-stearoyl-2-docosahexaenoyl-*sn*-glycero-3-phosphoethanolamine (SDPE)/cholesterol), and was simulated for over 1.5 μs following retinal isomerization to correspond to the Meta I state [55]. A case clearly supporting the complex-counterion model emerged from this line of research. Theoretical ^{2}H NMR spectra for the C5-, C9-, and C13-methyl groups of retinal were calculated from the final 500 ns of each MD trajectory, representative of the preactivated Meta I state (Figs. 2c,d). Calculations involved weighting the spectra with bond orientational distributions, and using a Monte Carlo method to compute results for a static uniaxial distribution with mosaic spread. Furthermore, calculations were performed for three sample alignments ($\theta = 0$, 45, and 90°) with respect to the magnetic field $\mathbf{B}_0$. Using different sample tilt angles allows for a more accurate and complete interpretation of the spectral data. Another factor to consider is the mosaic spread of the NMR samples: its contribution to the line shape is minimized close to 0°, meaning a more accurate result is produced. Clearly, there is a discrepancy between the experimental spectra of the Meta I state and the counterion-switch simulation (Fig. 2c), especially for the C9- and C13-methyl groups. This poor agreement occurs most evidently for the 0° tilt. In contrast, the complex-counterion model shows excellent agreement with the ^{2}H NMR data for Meta I (Fig. 2d), supporting this mechanism under which PSB deprotonation occurs subsequently in the active Meta II state [55].

By directly computing experimental observables, in this case the solid-state ^{2}H NMR spectral line shape, one can begin to appreciate the importance and complementary nature of experimental and computational techniques. Successfully duplicating experimental data also allows one to interpret other aspects of simulation results, such as dihedral fluctuations in the retinal polyene chain. Lastly, one is able to draw parallels between rhodopsin and other GPCRs that are activated by diffusible ligands.

4. Solid-state ^{2}H NMR spectroscopy investigates the dynamics of cofactors bound to membrane proteins

We have emphasized above that solid-state NMR spectroscopy is an invaluable tool to study the structure and dynamics of membrane proteins, inasmuch as the proteolipid system cannot be dissolved and investigated by solution NMR. In particular, solid-state NMR line shapes entail structural restraints involving residual dipolar couplings (RDCs) or residual quadrupolar couplings (RQCs) (the former are related to internuclear distances and the latter to bond angles). Moreover, NMR relaxation provides unique information on molecular motions, and reveals intra- and intermolecular interactions through dynamical parameters. Specific interactions are further investigated by combining relaxation data with structural data.

4.1. Relaxation in ^{2}H NMR spectroscopy provides key insights into retinal mobility

The complementary nature of solid-state ^{2}H NMR spectral line shape and relaxation studies is illustrated in Fig. 3, which shows experimental results for rhodopsin in the dark state with retinal ^{2}H-labeled at the C5-, C9-, or C13-methyl groups. Data are included for rhodopsin in unoriented recombinant membranes comprising 1-palmitoyl-2-oleoyl-*sn*-glycero-3-phosphocholine (POPC). The RQCs obtained from the powder-type spectra (Figs. 3a–c) show that the amplitude of the fluctuations of the retinal methyl groups describe the dynamic structure of retinal embedded in the binding pocket of rhodopsin. The average structure of retinal is characterized by the order parameter $S_{C_3} = \frac{1}{2}\langle 3\cos^2\beta_{IM} - 1\rangle$ of the various methyl groups. Here β_{IM} is the angle between the instantaneous C–C^{2}H$_3$ axis direction (I) and the average methyl group (M) orientation. The residual quadrupolar splittings for the C5-, C9-, and C13-methyl groups indicate motional narrowing, due to rapid spinning of the methyl groups about their C_3 axes. Comparing the residual (motionally averaged) quadrupolar coupling $\langle\chi_Q\rangle$ with the value of χ_Q due to fast spinning of the methyl group yields $S_{C_3} \approx 0.9$, representing an amplitude of the off-axial fluctuations of $\Delta\beta_{IM} \approx 15°$. Note that this motion includes both methyl group fluctuations with respect to the unsaturated polyene, as well as any reorientations of the retinal ligand within the binding pocket of rhodopsin. Because the solid-state ^{2}H NMR spectra are in the fast motional limit, they do not distinguish among the various possible contributions to the methyl group dynamics. However, site-specific differences in retinal methyl mobility can be delineated from partially-relaxed ^{2}H NMR spectra, as well as from the inversion–recovery curves used to establish the spin–lattice relaxation times (Figs. 3d–f).

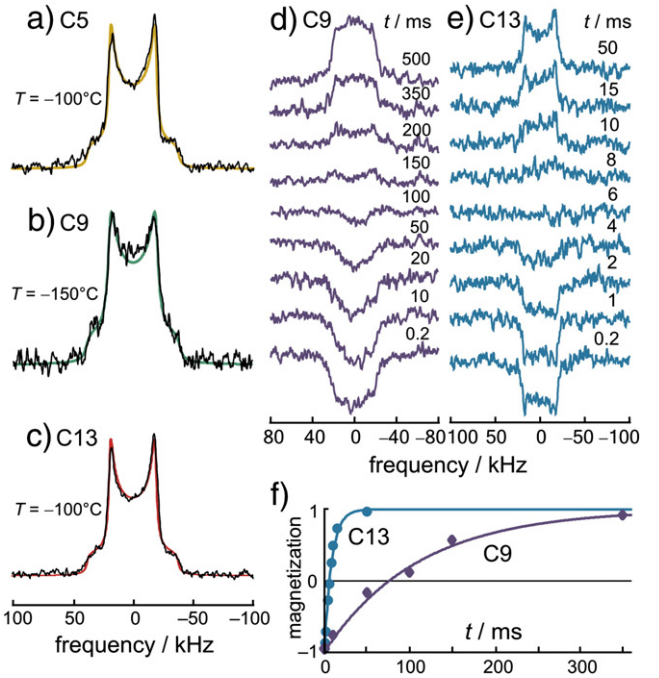

Fig. 3. Site-specific ^{2}H NMR relaxation manifests functional dynamics of retinal methyl groups within the ligand-binding cavity of rhodopsin. (a–c) Powder-type ^{2}H NMR spectra of rhodopsin containing 11-*cis*-retinal with ^{2}H-labeled C5-, C9- or C13-methyl groups in POPC bilayers (1:50 protein to lipid molar ratio). Solid-state ^{2}H NMR line shapes demonstrate rapid spinning of C–C^{2}H$_3$ groups at temperatures down to at least −160 °C. (d, e) Inversion-recovery ^{2}H NMR spectra for retinylidene C9- and C13-methyl groups of rhodopsin in aligned POPC membranes at −150 °C. The tilt angle θ between the average membrane normal and magnetic field is equal to 0°. (f) Inversion-recovery plots for C9- and C13-methyl groups at −150 °C demonstrate site-specific variations in longitudinal Zeeman (T_{1Z}) relaxation times.
Figure adapted with permission from Ref. [35].

To further elucidate how the retinal dynamics are implicated in rhodopsin function, we measured ^{2}H relaxation times (Zeeman, T_{1Z}, and quadrupolar order, T_{1Q}) for aligned or nonaligned (powder-type) samples (Fig. 4). Data were acquired in the temperature range from −30 to −160 °C (close to values used for X-ray [56] and spin-label EPR [23] studies), which is well below the melting temperature (T_M) of the lipid bilayer. Working below T_M freezes out the rotational diffusion and large-scale (collective) motions of rhodopsin, and allows us to focus on the internal (local) dynamics of retinal. This approach constitutes a rather different strategy from that typically employed in solution NMR of proteins [57]. Moreover, the lipid dependence of rhodopsin intermediates [58–61] was used to quantitatively trap the Meta I and Meta II photoproducts in frozen aligned rhodopsin films.

Now in the partially-relaxed ^{2}H NMR spectra (Figs. 3d,e), the null point for inversion recovery is related to T_{1Z} by $t = T_{1Z}\ln 2$. As a result, by comparing the data for the C9- and C13-methyl groups, we can immediately see that the spin–lattice relaxation rates differ by more

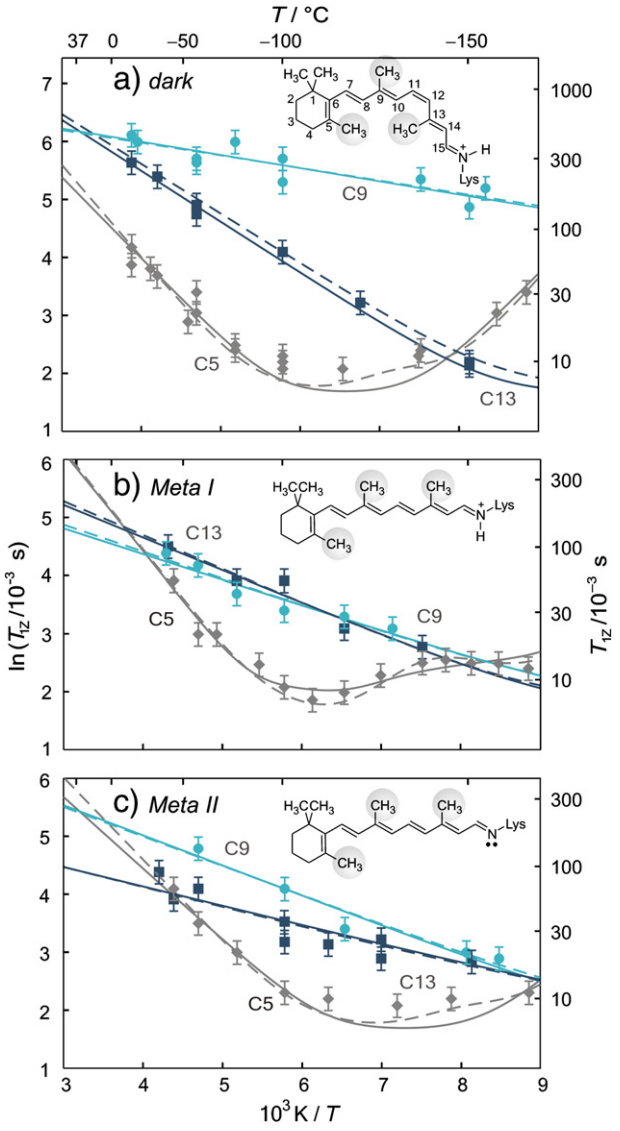

Fig. 4. Solid-state ^{2}H NMR relaxation uncovers striking changes in retinal mobility and interactions during rhodopsin activation. (a–c) Spin–lattice (T_{1Z}) relaxation times of retinylidene methyl groups were measured in (a) the dark state, (b) the Meta I state, and (c) the Meta II state at temperatures ranging from −30 to −160 °C. Methyl dynamics were analyzed using either an axial 3-fold jump model, or a continuous diffusion model with coefficients $D_{||}$ (for methyl group rotation about the 3-fold (C_3) symmetry axis) and $D_{\perp}$ (for methyl axis reorientation). In panels (a–c) an axial 3-fold jump model or a continuous diffusion model with $D_{\perp}=0$ are represented by solid lines; the dashed lines are for a continuous diffusion model having restricted off-axial diffusion with $D_{\perp}=D_{||}$. In panel (b) theoretical fits for the C5-methyl group in Meta I assume either two conformers with different bond orientations and axial diffusion coefficients (solid line), or two different rotational diffusion constants ($D_{||}\neq D_{\perp}$) (dashed line).
Figure adapted with permission from Ref. [35].

than an order of magnitude (Fig. 3f). This variation is caused by site-specific differences in the intramolecular dynamics of the retinylidene chromophore. Since the RQCs for the retinal methyl groups are nearly equivalent, the relaxation differences must arise from the methyl spinning rates, as opposed to the amplitude of the off-axial motions (S_{C_3}). What becomes clear is that distinct variations exist in the internal mobility of the retinal methyl groups in the dark state [35]. The T_{1Z} relaxation times for the dark, Meta I, and Meta II states increase with temperature for each of the methyl groups, except for the C5-methyl at extremely low temperatures. This means that motional correlation times are less than $1/\omega\approx 2$ ns except for the C5-methyl group, whose experimental rotational correlation time exceeded 2 ns below approximately −120 °C. (In Ref. [35] the value of $1/\omega\approx 13$ ns is a misprint and should be corrected as indicated here.)

The ^{2}H NMR relaxation results are summarized in Fig. 4, which shows Arrhenius-type plots of the T_{1Z} relaxation times versus inverse temperature in the dark, Meta I, and Meta II states, respectively. A minimum is expected in plots of ln T_{1Z} versus $1/T$, since matching the power spectrum (i.e. spectral density) of the fluctuations to the energy level transitions is optimal when the correlation time is near the inverse resonance (Larmor) frequency. Consequently, shifting the minimum to lower temperature corresponds to faster motions and vice versa. Quantitative evaluation assumes transition state theory leading to $A\exp(-E_a/RT)$ for the temperature dependence. Here the preexponential factor A represents the intrinsic rate of rotation in the absence of a barrier, i.e. $E_a<<RT$ corresponding to infinite temperature, where E_a is the barrier height (activation energy) for the methyl rotation [34]. The width of the minimum in the ln T_{1Z} versus $1/T$ plot is inversely related to the E_a activation barrier for the methyl dynamics. For temperatures significantly above the T_{1Z} minimum, the plot essentially corresponds to an Arrhenius-type law, where the slope is proportional to E_a (see below).

4.2. Methyl groups probe site-specific local interactions in the inactive dark state

Keeping in mind that ^{2}H NMR relaxation can provide us with site-specific variations in retinal mobility, we are now able to examine the behavior of ^{2}H-labeled retinal bound to rhodopsin in the inactive dark state. Fig. 4a shows that ln T_{1Z} has a temperature dependence that is nearly linear for the C9- and C13-methyl groups, although with quite different slopes. By contrast, a curve with a minimum near −120 °C is observed for the C5-methyl group. Hence, the individual methyl groups possess markedly different dynamical and relaxation behavior, with three nonequivalent environments in the dark state. Smaller T_{1Z} values and rotational diffusion coefficients are correlated to larger activation energy (E_a) values and vice versa, which may indicate a role of nonbonded interactions. Other differences originate from the preexponential factor: for instance, the T_{1Z} value for the C9-methyl at the higher temperature (Fig. 4a) is due to a relatively small preexponential factor, as opposed to the activation energy.

These differences in the rotational dynamics and activation energies of the methyl groups observed in the dark state (and upon transition to the Meta I and Meta II states, see below) can be attributed to a combination of intra- and intermolecular interactions of retinal within the chromophore binding pocket. The dynamical parameters obtained from Fig. 4a indicate that at low temperatures (<0 °C), the β-ionone ring (C5-methyl group) is the least mobile in the dark state. In addition, the C13-methyl group of the polyene chain has intermediate mobility, and the C9-methyl in the middle of the retinylidene cofactor is most mobile. Despite different temperature dependencies and E_a values, the mobility of the C9- and C13-methyl groups is almost the same near physiological temperature. By contrast, the T_{1Z} time for the C5-methyl and correspondingly its rate of motion are ≈3-fold smaller (see below).

Another interesting observation from the relaxation data in the dark state (Fig. 4a) is that the C9-methyl activation energy is significantly less than for the C5- and C13-methyl groups. A possible explanation is that the C9-methyl group dynamics are strongly determined by 1–6 interactions (C9-methyl hydrogen to H7 and C9-methyl hydrogen to H11), which can be approximated by 3-fold rotational potentials. Although these potentials may be the same order of magnitude as 1–7 interactions (C13-methyl hydrogen to H10), they are shifted with respect to each other by ≈60°, thus producing a shallow potential and activation energy. This hypothesis is further supported by quantum mechanics (QM) calculations (see below). As a result, we propose that nonbonded 1–6 intramolecular interactions are the primary reason for the low activation energy E_a and also the relatively small preexponential factor for 3-fold jumps of the C9-methyl group. According to the X-ray

structure [5] and MD simulations [62], the dynamics of both the C9- and C13-methyl groups are most likely relatively unaffected by intermolecular interactions in the dark state; on average, these groups are ≥4 Å away from amino acid side chains. It follows that the activation energy for the C13-methyl rotational diffusion is mainly determined by the nonbonded 1–7 interaction with hydrogen H10. The high activation energy for the C5-methyl group in the dark state stems from interactions with hydrogen H8 of the retinal ligand and the Glu^{122} side chain. This proposal is consistent with a Fourier transform infrared (FTIR) study of desmethyl and acyclic analogs of retinal bound to rhodopsin [63], and is supported by close proximity of the C5-methyl group to Glu^{122} in the X-ray crystal structure [5].

4.3. Changes in retinylidene methyl dynamics occur in the preactive Meta I state and signaling Meta II state

It is striking that compared to the dark state (Fig. 4a) significant differences occur in the relaxation behavior for the C5- and C9-methyl groups in the Meta I and Meta II states (Figs. 4b, c). The E_a for the crucial C9-methyl group (3.7 kJ mol^{-1}) is markedly increased (by a factor of ≈2) in Meta I, up to a level similar to the C13-methyl. Concurrently, the E_a value for the C13-methyl group in the Meta I state (4.7 kJ mol^{-1}) is reduced by about one-third, making its T_{1Z} values nearly identical to those of the C9-methyl group. The decreased C9-methyl mobility following isomerization is most likely related to the more crowded environment, which results from the polyene chain all-*trans* conformation and nonbonded interactions within the binding pocket of rhodopsin. The lack of high-resolution Meta I structural data makes it difficult to identify which specific amino acids affect the C9-methyl mobility, which could potentially explain changes in its activation energy. As mentioned previously, the reduction of the activation energy for the C13-methyl group (from 7.3 to 4.7 kJ mol^{-1}) makes sense, because the 11-*cis*→all-*trans* isomerization places the C9- and C13-methyl groups on the same side of the molecule (Fig. 4). Hence they undergo similar intramolecular interactions, and experience a similar mobility.

Interestingly, changes are also observed in the T_{1Z} values for the C5-methyl group in Fig. 4, with an emergence of a second temperature-dependent minimum in the Meta I state, and subsequent reversion to a single minimum in the Meta II state. The significance of the T_{1Z} minimum is that the relaxation time at this temperature unequivocally defines the effective correlation time, as described below. Evidently the C5-methyl relaxation data in the Meta I state do not conform to the framework of a 3-fold jump model with a single E_a value. The two minima may represent two distinct types of motion, e.g. methyl group rotation and β-ionone ring reorientation. An alternative interpretation would be the presence of two 6-*s*-*cis* conformers of the retinal, with positive and negative torsion angles for the C6–C7 bond [62].

Regardless of the model used to describe the C5-methyl dynamics, its behavior remains similar in both the dark and Meta I states. The rotational dynamics are dramatically slower, and the activation energy E_a for the C5-methyl (>10 kJ mol^{-1}) is much larger compared to the C9- and C13-methyl groups (Fig. 4). Furthermore, the minimum of the C5-methyl T_{1Z} temperature dependence occurs at an elevated temperature versus the C9- and C13-methyls. This essentially means that the C5-methyl rotation is restricted in the dark and Meta I states. It has been proposed recently that the β-ionone ring and, in particular, the C5-methyl disrupts the hydrogen bonding network around Glu^{122} in the Meta I→Meta II transition, due to retinal motion toward helix H5 [63,64]. This movement of the β-ionone ring has been regarded as an essential part of the rhodopsin activation mechanism. In this respect, the existence of two minima in the T_{1Z} temperature dependence may indicate a more restricted environment for C5-methyl group rotation in the Meta I state versus the dark state.

Another important finding of this work is that relatively small changes occur in the retinal dynamics upon the transition from the Meta I to the Meta II state. The E_a values and rotational diffusion constants increase slightly for the C9-methyl group (from 3.7 to 4.3 kJ mol^{-1}) and decrease for the C13-methyl (from 4.7 to 2.8 kJ mol^{-1}) (Fig. 4c). The E_a value for the C13-methyl group progressively decreases from the dark state to Meta I, and then to the Meta II state. This is the result of a stepwise decrease of the preexponential factor from state to state during the activation process of rhodopsin. For the C5-methyl group, the minimum observed in the T_{1Z} temperature dependence shifts to lower temperature on going from the dark to the Meta II state (E_a = 10.3 kJ mol^{-1}). This position approximately corresponds to the average of the two minima in the Meta I state. The minimum also broadens, which would indicate a superposition of two nearby minima. Most striking, the overall T_{1Z} temperature dependence for the C5-methyl in the dark, Meta I, and Meta II states remains the same (differences in E_a barely exceed 20% for a given model of the rotational dynamics), implying a stable environment for the β-ionone ring. A similar conclusion has been reached based on ^{13}C chemical shift data [64,65].

5. Analytical relaxation theory and numerical dynamics simulations characterize the energy landscape of rhodopsin activation

As a rule there are two approaches to the quantitative analysis of NMR relaxation data, such as those summarized above. First, one can employ the general theory of nuclear spin relaxation to interpret the relaxation times in terms of the power spectral densities and correlation functions, using simplified models for the rotational dynamics in analytical closed form. Alternatively, we can forgo an exact mathematical description, and interpret the experimental relaxation times using numerical molecular dynamics simulations. Here the temporal evolution of the molecular positions and orientations under the influences of a force field encapsulates knowledge of intra-and intermolecular interactions pertinent to the systems under investigation. Both approaches are valid, because their characteristic strengths and weaknesses are different and tend to be complementary.

5.1. Solid-state ^2H NMR highlights the functional motions of retinal methyl groups

According to theory, the ^2H NMR relaxation rates are determined by the power spectrum (spectral density) of the thermal fluctuations of the quadrupolar coupling tensor near the resonance frequency [66]. They are given by

$$R_{1Z} = 1/T_{1Z} = \tfrac{3}{4}\pi^2\chi_Q^2[J_1(\omega_0) + 4J_2(2\omega_0)] \quad (1)$$

and

$$R_{1Q} = 1/T_{1Q} = \tfrac{9}{4}\pi^2\chi_Q^2 J_1(\omega_0), \quad (2)$$

where χ_Q is the static quadrupolar coupling constant, and ω_0 is the resonance (Larmor) frequency. Here $J_m(m\omega_0)$ denotes the spectral density (m = 1,2), which is a function of the molecular geometry, the mean-square amplitudes of the motion, and the rotational correlation times (τ_r). The latter in turn are related to the rate constant for 3-fold rotations (k) about the C_3 methyl axis by $1/\tau_r = 3k$ (r = 1) [39]. An alternative approach is to use a continuous rotational diffusion model [66]. Within a strong collision approximation one obtains $1/t_r \approx 6D_\perp + (D_{||} - D_\perp)r^2$, where the rotational diffusion coefficients $D_{||}$ and $D_\perp$ characterize methyl group axial rotation and off-axial fluctuations, correspondingly. The temperature dependence of either

the jump rate or rotational diffusion constants assumes an Arrhenius law, as described above (cf. [34] for detailed description).

In principle, T_{1Z} measurements at different orientations for aligned samples or at different frequencies for powder-type samples allow one to identify specific motional mechanisms. An axial jump model predicts a ≈20% difference in the methyl relaxation depending on orientation [67], whereas for an axial diffusion model the methyl relaxation is angular independent [39,66]. In practice, for the case of powder-type samples our T_{1Z} measurements were limited to the $\theta = 90°$ orientation of the methyl axis to the main magnetic field $\boldsymbol{B}_0$, due to the relatively low signal-to-noise ratio. Aligned samples were investigated at the $\theta = 0°$ orientation relative to $\boldsymbol{B}_0$. There was no detectable difference in the relaxation times for various orientations. Consequently, the experimental error of the T_{1Z} measurements (about 10%) did not allow us to make unambiguous conclusions about the reorientation mechanism. Both a 3-fold jump [67] and a continuous diffusion [66] model were used to fit the temperature dependence of the T_{1Z} and T_{1Q} relaxation times (Fig. 4). For the dark, Meta I, and Meta II states of rhodopsin, the T_{1Z} data could be fit with a 0:1 $D_\perp/D_\parallel$ ratio to within experimental error. However, simultaneous fitting of the T_{1Z} and T_{1Q} temperature dependencies could only be performed for $D_\parallel = 0$ (results not shown), meaning that methyl group off-axial fluctuations are much slower than spinning about its 3-fold symmetry axis. The preexponential factor and E_a values obtained using transition state theory (see above) vary according to the model, yet the qualitative picture remains the same.

5.2. Molecular dynamics simulations expand the ^{2}H NMR results to longer time scales

For rhodopsin proteolipid membranes, molecular dynamics (MD) simulations offer the ability to study both smaller (ns) and larger (μs) time-scale dynamics for the entire system, providing the basis for extending insights from ^{2}H NMR spectroscopy. Many system aspects can be examined: protein–lipid interactions [49,50], behavior of the lipid bilayer (i.e., bilayer thickness, order parameters, lipid diffusion, etc.) [68], protein conformational changes leading to the activated state [43,62,69], and agonist binding effects [17]. However, two limitations need to be considered when modeling GPCRs: (*i*) the inaccessibility of longer time scales (rhodopsin reaches Meta II in milliseconds) and (*ii*) the use of an empirically derived molecular mechanics (MM) force field to approximate atomic interactions. Clearly, molecular mechanics force fields are intended to correctly reproduce experimental phenomena. Because they are empirically derived, however, MM force fields are continually improved as experimental data and theory become more robust. This applies especially to retinal, since our latest ^{2}H NMR research clearly shows that each methyl group has site-specific intra- and intermolecular interactions (Fig. 4). Addressing this issue is biologically important, because experiment has shown that the retinal methyl groups are essential to rhodopsin activation [63,70]. As a result, we have used ab initio quantum mechanics calculations to examine the applicability of MM force fields for describing the rotational behavior of methyl groups in appropriate retinal model compounds.

6. Quantum mechanical calculations address methyl dihedral terms in the retinal force field

In molecular mechanics, the force field encapsulates all information about the intra- and intermolecular forces that act upon the molecular system of interest. Analysis of bond angle bending, stretching, and torsions as well as electronic structure requires knowledge of intramolecular potential energies that derive ultimately from either quantum mechanical calculations or experimental data. For molecules such as retinal, a current drawback is that they are too large to be accurately computed with high-level quantum theory. Calculations must be restricted to comparatively small fragments that approximate the molecular orbitals. Here, recent advances in computing power have motivated us to reexamine the torsional potential energy terms for retinal currently used with CHARMM and other molecular mechanics programs. Our general aim is to more accurately model experimental ^{2}H NMR relaxation data for rhodopsin in different functional states.

6.1. Larger polyene compounds are necessary to model the retinylidene methyl groups

Comparison of our ^{2}H NMR results with functional data [63,70] has demonstrated that each of the retinylidene methyl groups contributes individually and uniquely to rhodopsin activation. This finding is in agreement with several FTIR studies conducted on retinal desmethyl analogs, which show that removal of any methyl group prevents rhodopsin from becoming fully activated [63,70]. In contrast, previous MD simulations of the rhodopsin proteolipid system have neglected the retinal methyl torsion force constants by setting them to zero [71] (i.e. the potential energy was assumed to be determined solely by nonbonded terms). The discrepancy between experiment and simulation led us to a closer examination of the methyl dihedral parameters in the retinal force field (Fig. 5). The majority of molecular mechanics force fields draw from a combination of experimental and theoretical data to create a set of parameters that are used to solve Newton's equations of motion. In the case of retinal methyl dihedrals, quantum mechanical calculations (in this case, MP2 level of theory with a 6–31 G** basis set) are employed to formulate the force field parameters.

When examining retinal methyl rotations, steric interactions with the polyene chain figure prominently. Specifically, methyl groups in an all-*trans* polyene chain experience 1–6 interactions

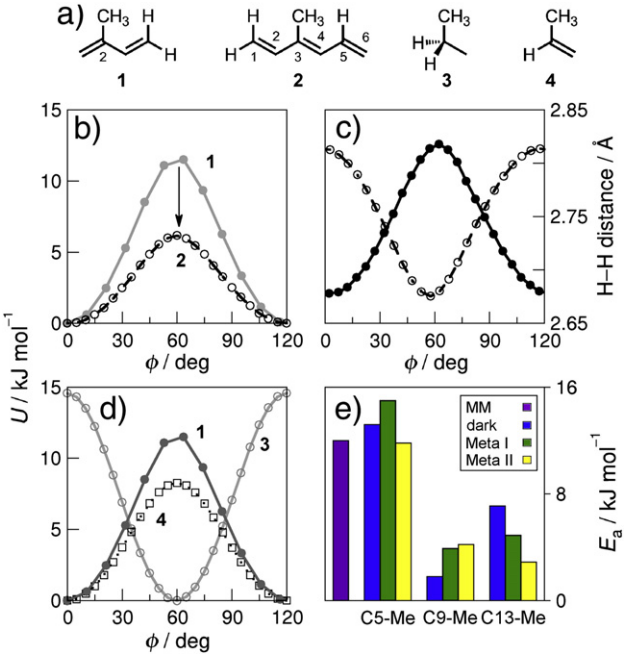

Fig. 5. Quantum mechanical theory reveals the influences of steric interactions on torsional potential energy surfaces underlying retinal methyl rotation. (a) Model compounds corresponding to fragments of retinal used for QM calculations. (b) Comparison of QM (circles) and MM (lines) energies plotted against methyl torsion angle (ϕ) for 2-methyl-butadiene (2MBD) (compound **1**) and 3-methyl-hexatriene (3MHT) (compound **2**). (c) Plot of 1–6 distance in 3MHT between methyl hydrogen and C1 vinyl hydrogen (closed) and C5 vinyl hydrogen (open). (d) Plot of QM energy as a function of methyl torsion angle in 2MBD (compound **1**), propane (compound **3**), and propene (compound **4**). (e) Activation energies (E_a) for C5-, C9-, and C13-methyl groups obtained from ^{2}H NMR data for the dark, Meta I, and Meta II states of rhodopsin versus standard MM dihedral energy barrier in CHARMM force field.
Figure adapted with permission from Ref. [72].

between the methyl hydrogens and those hydrogen atoms bound to neighboring vinyl groups. For 2-methyl-butadiene (2MBD) (compound **1**), the largest polyene fragment currently used in the retinal force field distributed with CHARMM, only one such 1–6 interaction is present (Fig. 5a). By extending the polyene chain by two carbons, creating the fragment 3-methyl-hexatriene (3MHT) (compound **2**), we now possess a methyl group with two 1–6 interactions. Adding the extra 1–6 interaction reduces the 3MHT methyl energy barrier in comparison to 2MBD by raising the energies of both the minimum energy conformation and the eclipsed state (Fig. 5b). For 3MHT the 1–6 interhydrogen distances as a function of torsion angle also demonstrate the effect of dual 1–6 interactions (Fig. 5c), showing that 3MHT is nearly symmetrical over the course of a methyl rotation. The distance between the methyl group and the C1 vinyl hydrogen (direction of single bond) is slightly higher at its point of closest approach than the corresponding distance to the C5 vinyl hydrogen (direction of double bond). Hence, the steric repulsion at the torsional energy maximum is slightly greater than the repulsion at the minimum.

These results suggest that 3MHT is the smallest possible fragment to accurately model the retinal C9-methyl group. The standard parametrization procedure is to fit the QM results to the torsional energy term in the molecular mechanics force field. For the MM package CHARMM, this contribution takes the form $U(\phi) = K_\phi[1 + \cos(n\phi + \delta)]$. By retaining the current force field terms—and using a new dihedral potential—one can perform MM simulations of the polyene fragments 2MBD and 3MHT and compare the results to QM calculations (Fig. 5b). It can be seen that the new dihedral parameters accurately reproduce the QM rotational profile, and give a marked improvement in the retinal force field.

6.2. Hyperconjugation extends to methyl groups of the retinal chromophore implicated in rhodopsin activation

One should note that polyene chains have unique covalent bond characteristics, due to their single bond-double bond alternation. This bond alternation creates hyperconjugation effects, which essentially imparts shared single and double bond properties to each bond in the polyene chain. In order to fully understand the steric effects on 2MBD and 3MHT, it was necessary to examine two smaller model compounds, propane (compound **3**) and propene (compound **4**), Fig. 5a. The QM results show that the methyl rotation barrier of a fully saturated hydrocarbon chain (propane) is not necessarily equivalent to the same barrier of an unsaturated chain (propene), shifting both the barrier location and height (Fig. 5d). In addition, the methyl rotational barrier of propene is almost half (8 kJ mol^{-1}) that of propane (15 kJ mol^{-1}), which stems from different orbital interactions in these two molecules. The most stable methyl conformation in propene is at $\phi = 0°$, where the methyl C–H bond is *cis* to the vinyl C═C bond. The reason for this stability is hyperconjugation: the other two methyl hydrogens are connected by a vector perpendicular to the C═C bond axis, which involves stabilization through interaction of the filled π-like CH_2 orbitals of the methyl group and the unoccupied π^* molecular orbital of the double bond. Propane lacks these hyperconjugative interactions, with the most stable conformer being the staggered orientation.

In the context of 2MBD and 3MHT, the dramatically increased rotational barrier of 2MBD compared to propene (Fig. 5d) is due to steric repulsion between the methyl and vinyl hydrogen atoms, which is maximized for 2MBD when both hydrogen atoms are eclipsed. Because of the 3-fold symmetry of the methyl group, when one of the methyl hydrogens is eclipsed ($\phi = 180°$), the other methyl hydrogens lie at 60°. Thus maximum steric repulsion coincides with the highest energy state arising from orbital interactions, with the net effect of raising the energy barrier by ≈50% in 2MBD compared to propene (Fig. 5d). This steric effect would predict a rotational barrier for 3MHT that is slightly higher than propene, while QM calculations give the opposite (Figs. 5b,d). Most likely, this discrepancy stems from the altered π orbital characteristics when increasing polyene chain unsaturation from one double bond (propene) to three (3MHT). Yet another hyperconjugation effect, which was not considered in our original ^{2}H NMR analysis [21], but which came to light in our theoretical investigations [72], was that protonation of the Schiff base yields a lowering of the C13-methyl rotational energy barrier. This finding is significant due to the fact that Meta II involves deprotonation of the PSB, which in an MD simulation would involve physically removing the proton from the terminus of retinal. Currently these time scales are not attainable—but with advances in computational power, and the availability of new crystal structures in putative Meta II states [9,10], they will be soon.

These QM calculations, guided by insight from experiment, ultimately led to improvements in the retinal force field [72]. Direct comparisons between the ^{2}H NMR data and QM results cannot be made, since the experimental analysis is made in the protein environment and the theoretical analysis is made in vacuo. However, it is clear from both approaches that intramolecular steric clashes with hydrogens play a large role in determining the activation energy profiles for retinal methyl rotations. The effort put into the analysis of such a small molecular component of the rhodopsin system, viz. retinal, is important due to the crucial role it plays in rhodopsin activation. An improved MM force field will thus allow future investigations of effective barrier heights in the full protein environment, with subsequent quantitative comparisons and detailed interpretations of experimental observations.

7. Putting it all together: the rhodopsin activation mechanism

Based on the structural [11,12,20,23,65,73–76] and dynamical [34,35,45,46,49,55,62] data, a multiscale activation mechanism has been proposed, whereby retinal isomerization initiates collective helix fluctuations in the Meta I–Meta II equilibrium with multiple activated substates. The proposed structural changes upon rhodopsin activation are shown in Fig. 6. In accord with our MD simulations (ns time scale) [68], helices H1–H4 constitute the transmembrane core of the receptor, whereas the cytoplasmic loops evince significant motions [68]. Rhodopsin activation is due to movements of helices H5 and H6 together with H7. In an expanded view of the photopathway (Fig. 1), the early photointermediates (photorhodopsin, bathorhodopsin, BSI, lumirhodopsin) are followed by the major reactions [77]: Meta I ⇄ Meta II_a ⇄ Meta $II_b + H_3O^+$ ⇄ Meta II_bH^+; here Meta II_b and Meta II_bH^+ are the active conformational substates. The entropy-stabilized Meta II_b substate is in equilibrium with the Meta II_bH^+ substate, whose formation is enthalpically downhill [78]. Using ^{2}H NMR, we are able to show how the fast time-scale motions of retinal (ps) correspond to the helical movements associated with rhodopsin activation [35].

7.1. Retinal methyl groups assist in driving multiscale rhodopsin activation

In the dark state, the low activation barrier of the C9-methyl group ($E_a = 1.4$ kJ mol^{-1}) indicates the absence of steric clashes within the ligand-binding cavity of rhodopsin (see Figs. 4a, 5e). The small increase in E_a value for the C9-methyl in the Meta I state (from 1.4 to 3.7 kJ mol^{-1}) signifies the local environment changes following isomerization. Consequently, the ^{2}H NMR data suggest that leading up to and including the Meta I state [19], the C9-methyl acts effectively as a hinge point for retinal isomerization, causing reorientation of the C13-methyl and the C═NH^+— groups. Rotation of the C13-methyl group and the PSB occurs toward the C9-methyl group rather than vice versa. This conclusion is supported by the crystal structures of batho- and lumirhodopsin [8]. The reduced C13-methyl activation energy in Meta I suggests the second extracellular (E2) loop and the retinal ligand move apart. Hence, the C13-methyl rotation displaces the β_4 strand of the E2 loop toward the extracellular side, disrupting the hydrogen-bonding network connecting the extracellular ends of helices H4, H5, and H6 [20]. At the opposite end of retinal, the β-ionone ring is displaced toward the H3–H5 helical

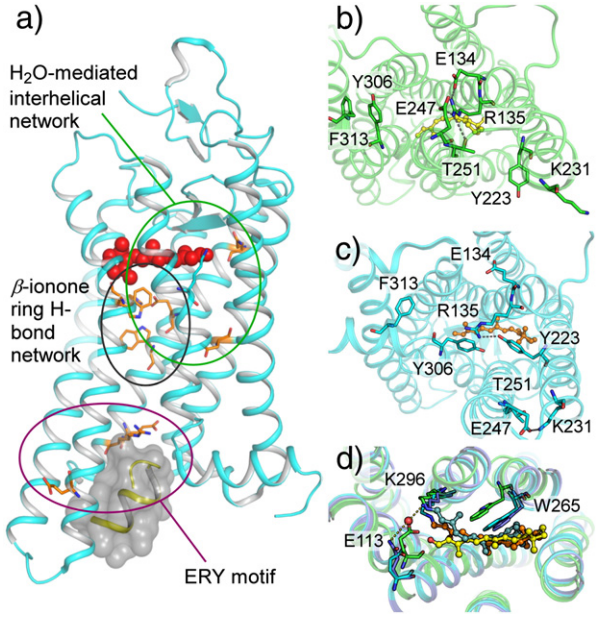

Fig. 6. Rhodopsin activation is triggered by retinal isomerization and stabilized by rearrangement of ionic locks. (a) Structure of rhodopsin (PDB accession number 2X72) shows hydrogen-bonding networks and ionic locks that rearrange or form after isomerization of the covalently bound retinal ligand. Spheres represent retinal; the sticks indicate residues in specific networks; the smooth van der Waals surface shows a transducin peptide fragment; and the ribbons depict the rhodopsin polypeptide backbone. (b) Rhodopsin in the dark state (PDB 1GZM) is stabilized by an ionic lock due to nonbonded interactions among Glu^{134}, Arg^{135}, and Glu^{247} residues. (c) Upon retinal isomerization the rearrangement of the ionic lock entails new interactions between Arg^{135}–Tyr^{223} and Glu^{247}–Lys^{231}–Thr^{251} (rhodopsin in putative Meta II state; PDB 2X72). (d) Comparison of ligand binding pocket for the dark state (PDB 1GZM; green sticks and cyan retinal), the E113Q putative Meta II state (PDB 2X72; purple sticks and yellow retinal), and for retinal-soaked opsin (PDB 3PQR; cyan sticks and orange retinal). Note that all-*trans*-retinal in the retinal-soaked opsin is rotated by ≈180° about its long axis either compared to 11-*cis*-retinal in the dark state or the E113Q mutant.

interface, producing increased packing for the C5-methyl as indicated by the relatively high E_a value in the Meta I state (Figs. 4b, 5e). Additionally, movement of the β-ionone ring rearranges the hydrogen-bonded network about Glu^{122} and His^{211} connecting helices H3 and H5 [30]. This releases allosteric constraints on helix H5, allowing it to rotate its cytoplasmic end toward helix H6. Retinal isomerization is thus responsible for transmission of energy against the E2 loop by the C13-methyl group, and toward helices H3 and H5 by the C5-methyl of the β-ionone ring. The ionic lock involving the retinylidene PSB on H7 with its complex counterion due to Glu^{113} (H3) and Glu^{181} (E2) is broken by internal proton transfer from the PSB to Glu^{113} in Meta II [52]. It follows that destabilization of the ionic lock may occur through the rotation of the C═NH^+— group due to retinal isomerization.

7.2. Ionic locks hold the key to rhodopsin–transducin interactions

Notably, retinal isomerization and the displacement of its PSB end away from the E2 loop create a potential steric clash of the middle of the polyene chain with Trp^{265} of H6. To avoid steric hindrance, Trp^{265} shifts toward helix H5 and in the cytoplasmic direction, enabling the concerted tilt of helix H6 away from the H1–H4 helical core (Fig. 6a). In addition to the PSB, a second ionic lock due to the E(D)RY motif is implicated with rhodopsin activation (Fig. 6b). Displacement of helix H5 occurs concurrently with the tilt of helix H6, bringing Tyr^{223} closer to Arg^{135} and Lys^{231} near to Glu^{247} (Fig. 6c) [12]. The charge adduct due to Glu^{134}/Arg^{135} of the E(D)RY sequence in helix H3 with Glu^{247} of helix H6 rearranges in Meta II with Arg^{135}–Tyr^{223} and Glu^{247}–Lys^{231}–Thr^{251} interactions [9] (Fig. 6c). Thus a second ionic lock is broken, exposing transducin (G_t) recognition elements on the cytoplasmic side. Receptor activation culminates with protonation of Glu^{134} of the E(D)RY motif from the aqueous medium [78] (Fig. 6a).

Our proposed mechanism [35] varies somewhat from the recent X-ray structure attributed to Meta II [9]. The Meta II X-ray structure was obtained from opsin crystals soaked with all-*trans*-retinal, showing the ligand is rotated by ≈180° about its long axis compared to rhodopsin in the dark state (Fig. 6d) [9]. The retinal location is in agreement with most distance constraints obtained from dipolar-assisted rotational-resonance NMR spectroscopy [30]. However, the authors mention that some larger distance deviations may indicate the existence of different Meta II substates observed in the NMR and X-ray experiments. Moreover, the X-ray crystal structure of the E113Q/N2C/D282C triple mutant in the active state shows an orientation of the retinal ligand that is opposite from the retinal-soaked opsin structure [10]. It is possible that the rotated orientation of retinal in Meta II obtained by opsin regeneration may stem from the crystal soaking protocol. At this point, it cannot be concluded that a singular Meta II structure has been unequivocally established. On the other hand, various experimental structures of the active state support the possibility of multiple Meta II substates being present in the Meta I–Meta II equilibrium [35,75,78].

8. Moving forward

According to the above picture, receptor activation occurs as a dynamical equilibrium of substates—a striking example of how conformational entropy plays a role in GPCR biology and pharmacology. On the other hand, full characterization of the rhodopsin activation mechanism remains incomplete. In particular, the temporal sequence of the conformational changes is not completely established, and it is unclear when or whether long-axis rotation of the retinal takes place in the binding pocket. This confusion stems from the fact that the three-dimensional structures of metarhodopsin I and metarhodopsin II were obtained with moderately low resolution, yielding somewhat contradictory results. Consequently, these X-ray structures require further confirmation and refinement. A fundamental question will be to determine if there is a unique activated rhodopsin conformation, or whether receptor function entails a conformational ensemble triggered by photoisomerization of the retinal ligand. In this context, solid-state NMR and computational simulation continue to provide key insights, because they are able to examine the dynamics of rhodopsin activation. But what is exciting to us and other researchers is that development of new NMR methods and improved computational hardware and software expand the horizons for elucidating new aspects of membrane protein function. More than ten years ago the first crystal structure of rhodopsin was published—and just over five years ago, microsecond-time scale simulations were considered the state of the art. Currently there are over a dozen solved GPCR structures, and microsecond time scales are becoming much more common in simulations. The synergistic interplay in which experiment and simulation are used to examine rhodopsin activation will continue to answer many of the key questions about GPCR function as the field evolves in the future.

Acknowledgements

Research support from the U. S. National Institutes of Health (EY019614 to BM and EY012049 and EY018891 to MFB) and the U. S. National Science Foundation (MCB0950258 to SEF) is gratefully acknowledged.

References

[1] D. Filmore, It's a GPCR world, Mod. Drug Discovery 7 (2004) 24–28.
[2] J.W. Lewis, D.S. Kliger, Absorption spectroscopy in studies of visual pigments: spectral and kinetic characterization of intermediates, Methods Enzymol. 315 (2000) 164–178.

[3] M.F. Brown, Influence of nonlamellar-forming lipids on rhodopsin, Curr. Top. Membr. 44 (1997) 285–356.
[4] K. Palczewski, T. Kumasaka, T. Hori, C.A. Behnke, H. Motoshima, B.A. Fox, I. Le Trong, D.C. Teller, T. Okada, R.E. Stenkamp, M. Yamamoto, M. Miyano, Crystal structure of rhodopsin: a G protein-coupled receptor, Science 289 (2000) 739–745.
[5] T. Okada, M. Sugihara, A.-N. Bondar, M. Elstner, P. Entel, V. Buss, The retinal conformation and its environment in rhodopsin in light of a new 2.2 Å crystal structure, J. Mol. Biol. 342 (2004) 571–583.
[6] J.J. Ruprecht, T. Mielke, R. Vogel, C. Villa, G.F.X. Schertler, Electron crystallography reveals the structure of metarhodopsin I, EMBO J. 23 (2004) 3609–3620.
[7] H. Nakamichi, T. Okada, Crystallographic analysis of primary visual photochemistry, Angew. Chem. Int. Ed. 45 (2006) 4270–4273.
[8] H. Nakamichi, T. Okada, Local peptide movement in the photoreaction intermediate of rhodopsin, Proc. Natl. Acad. Sci. U.S.A. 103 (2006) 12729–12734.
[9] H.-W. Choe, Y.J. Kim, J.H. Park, T. Morizumi, E.F. Pai, N. Krauβ, K.P. Hofmann, P. Scheerer, O.P. Ernst, Crystal structure of metarhodopsin II, Nature 471 (2011) 651–656.
[10] J. Standfuss, P.C. Edwards, A. D'Antona, M. Fransen, G. Xie, D.D. Oprian, G.F.X. Schertler, The structural basis of agonist-induced activation in constitutively active rhodopsin, Nature 471 (2011) 656–660.
[11] P. Scheerer, J.H. Park, P.W. Hildebrand, Y.J. Kim, N. Krauβ, H.-W. Choe, K.P. Hofmann, O.P. Ernst, Crystal structure of opsin in its G-protein-interacting conformation, Nature 455 (2008) 497–502.
[12] J.H. Park, P. Scheerer, K.P. Hofmann, H.-W. Choe, O.P. Ernst, Crystal structure of the ligand-free G-protein-coupled receptor opsin, Nature 454 (2008) 183–187.
[13] V. Cherezov, D.M. Rosenbaum, M.A. Hanson, S.G.F. Rasmussen, F.S. Thian, T.S. Kobilka, H.-J. Choi, P. Kuhn, W.I. Weis, B.K. Kobilka, R.C. Stevens, High-resolution crystal structure of an engineered human β_2-adrenergic G protein-coupled receptor, Science 318 (2007) 1258–1265.
[14] D.M. Rosenbaum, V. Cherezov, M.A. Hanson, S.G.F. Rasmussen, F.S. Thian, T.S. Kobilka, H.-J. Choi, X.-J. Yao, W.I. Weis, R.C. Stevens, B.K. Kobilka, GPCR engineering yields high-resolution structural insights into β_2-adrenergic receptor function, Science 318 (2007) 1266–1273.
[15] S.G.F. Rasmussen, H.-J. Choi, D.M. Rosenbaum, T.S. Kobilka, F.S. Thian, P.C. Edwards, M. Burghammer, V.R.P. Ratnala, R. Sanishvili, R.F. Fischetti, G.F.X. Schertler, W.I. Weis, B.K. Kobilka, Crystal structure of the human β_2 adrenergic G-protein-coupled receptor, Nature 450 (2007) 383–387.
[16] S.G.F. Rasmussen, H.-J. Choi, J.J. Fung, E. Pardon, P. Casarosa, P.S. Chae, B.T. DeVree, D.M. Rosenbaum, F.S. Thian, T.S. Kobilka, A. Schnapp, I. Konetzki, R.K. Sunahara, S.H. Gellman, A. Pautsch, J. Steyaert, W.I. Weis, B.K. Kobilka, Structure of a nanobody-stabilized active state of the β_2 adrenoceptor, Nature 469 (2011) 175–180.
[17] D.M. Rosenbaum, C. Zhang, J.A. Lyons, R. Holl, D. Aragao, D.H. Arlow, S.G.F. Rasmussen, H.-J. Choi, B.T. DeVree, R.K. Sunahara, P.S. Chae, S.H. Gellman, R.O. Dror, D.E. Shaw, W.I. Weis, M. Caffrey, P. Gmeiner, B.K. Kobilka, Structure and function of an irreversible agonist-β_2 adrenoceptor complex, Nature 469 (2011) 236–240.
[18] V.-P. Jaakola, M.T. Griffith, M.A. Hanson, V. Cherezov, E.Y.T. Chien, J.R. Lane, A.P. Ijzerman, R.C. Stevens, The 2.6 angstrom crystal structure of a human A_{2A} adenosine receptor bound to an antagonist, Science 322 (2008) 1211–1217.
[19] A.V. Struts, G.F.J. Salgado, K. Tanaka, S. Krane, K. Nakanishi, M.F. Brown, Structural analysis and dynamics of retinal chromophore in dark and Meta I states of rhodopsin from ^{2}H NMR of aligned membranes, J. Mol. Biol. 372 (2007) 50–66.
[20] S. Ahuja, V. Hornak, E.C.Y. Yan, N. Syrett, J.A. Goncalves, A. Hirshfeld, M. Ziliox, T.P. Sakmar, M. Sheves, P.J. Reeves, S.O. Smith, M. Eilers, Helix movement is coupled to displacement of the second extracellular loop in rhodopsin activation, Nat. Struct. Mol. Biol. 16 (2009) 168–175.
[21] A.V. Struts, G.F.J. Salgado, M.F. Brown, Solid-state ^{2}H NMR relaxation illuminates functional dynamics of retinal cofactor in membrane activation of rhodopsin, Proc. Natl. Acad. Sci. U.S.A. 108 (2011) 8263–8268.
[22] S. Jäger, I. Szundi, J.W. Lewis, T.L. Mah, D.S. Kliger, Effects of pH on rhodopsin photointermediates from lumirhodopsin to metarhodopsin II, Biochemistry 37 (1998) 6998–7005.
[23] C. Altenbach, A.K. Kusnetzow, O.P. Ernst, K.P. Hofmann, W.L. Hubbell, High-resolution distance mapping in rhodopsin reveals the pattern of helix movement due to activation, Proc. Natl. Acad. Sci. U.S.A. 105 (2008) 7439–7444.
[24] M. Eilers, P.J. Reeves, W. Ying, H.G. Khorana, S.O. Smith, Magic angle spinning NMR of the protonated retinylidene Schiff base nitrogen in rhodopsin: expression of ^{15}N-lysine- and ^{13}C-glycine-labeled opsin in a stable cell line, Proc. Natl. Acad. Sci. U.S.A. 96 (1999) 487–492.
[25] P.J.E. Verdegem, P.H.M. Bovee-Geurts, W.J. de Grip, J. Lugtenburg, H.J.M. de Groot, Retinylidene ligand structure in bovine rhodopsin, metarhodopsin-I, and 10-methylrhodopsin from internuclear distance measurements using ^{13}C-labeling and 1-D rotational resonance MAS NMR, Biochemistry 38 (1999) 11316–11324.
[26] X. Feng, P.J.E. Verdegem, M. Edén, D. Sandström, Y.K. Lee, P.H.M. Bovee-Geurts, W.J. de Grip, J. Lugtenburg, H.J.M. de Groot, M.H. Levitt, Determination of a molecular torsional angle in the metarhodopsin-I photointermediate of rhodopsin by double-quantum solid-state NMR, J. Biomol. NMR 16 (2000) 1–8.
[27] A.F.L. Creemers, S. Kiihne, P.H.M. Bovee-Geurts, W.J. DeGrip, J. Lugtenburg, H.J.M. de Groot, ^{1}H and ^{13}C MAS NMR evidence for pronounced ligand–protein interactions involving the ionone ring of the retinylidene chromophore in rhodopsin, Proc. Natl. Acad. Sci. U.S.A. 99 (2002) 9101–9106.
[28] E. Crocker, M. Eilers, S. Ahuja, V. Hornak, A. Hirshfeld, M. Sheves, S.O. Smith, Location of Trp265 in metarhodopsin II: implications for the activation mechanism of the visual receptor rhodopsin, J. Mol. Biol. 357 (2006) 163–172.
[29] S. Ahuja, M. Eilers, A. Hirshfeld, E.C.Y. Yan, M. Ziliox, T.P. Sakmar, M. Sheves, S.O. Smith, 6-*s*-*cis* conformation and polar binding pocket of the retinal chromophore in the photoactivated state of rhodopsin, J. Am. Chem. Soc. 131 (2009) 15160–15169.
[30] S. Ahuja, E. Crocker, M. Eilers, V. Hornak, A. Hirshfeld, M. Ziliox, N. Syrett, P.J. Reeves, H.G. Khorana, M. Sheves, S.O. Smith, Location of the retinal chromophore in the activated state of rhodopsin, J. Biol. Chem. 284 (2009) 10190–10201.
[31] G. Gröbner, I.J. Burnett, C. Glaubitz, G. Choi, A.J. Mason, A. Watts, Observations of light-induced structural changes of retinal within rhodopsin, Nature 405 (2000) 810–813.
[32] G.F.J. Salgado, A.V. Struts, K. Tanaka, N. Fujioka, K. Nakanishi, M.F. Brown, Deuterium NMR structure of retinal in the ground state of rhodopsin, Biochemistry 43 (2004) 12819–12828.
[33] G.F.J. Salgado, A.V. Struts, K. Tanaka, S. Krane, K. Nakanishi, M.F. Brown, Solid-state ^{2}H NMR structure of retinal in metarhodopsin I, J. Am. Chem. Soc. 128 (2006) 11067–11071.
[34] M.F. Brown, G.F.J. Salgado, A.V. Struts, Retinal dynamics during light activation of rhodopsin revealed by solid-state NMR spectroscopy, Biochim. Biophys. Acta 1798 (2010) 177–193.
[35] A.V. Struts, G.F.J. Salgado, K. Martínez-Mayorga, M.F. Brown, Retinal dynamics underlie its switch from inverse agonist to agonist during rhodopsin activation, Nat. Struct. Mol. Biol. 18 (2011) 392–394.
[36] J.A. Barry, T.P. Trouard, A. Salmon, M.F. Brown, Low-temperature ^{2}H NMR spectroscopy of phospholipid bilayers containing docosahexaenoyl (22:6ω3) chains, Biochemistry 30 (1991) 8386–8394.
[37] K. Rajamoorthi, M.F. Brown, Bilayers of arachidonic acid containing phospholipids studied by ^{2}H and ^{31}P NMR spectroscopy, Biochemistry 30 (1991) 4204–4212.
[38] T.P. Trouard, T.M. Alam, M.F. Brown, Angular dependence of deuterium spin–lattice relaxation rates of macroscopically oriented dilaurylphosphatidylcholine in the liquid-crystalline state, J. Chem. Phys. 101 (1994) 5229–5261.
[39] A.A. Nevzorov, T.P. Trouard, M.F. Brown, Lipid bilayer dynamics from simultaneous analysis of orientation and frequency dependence of deuterium spin–lattice and quadrupolar order relaxation, Phys. Rev. E 58 (1998) 2259–2281.
[40] D. Otten, M.F. Brown, K. Beyer, Softening of membrane bilayers by detergents elucidated by deuterium NMR spectroscopy, J. Phys. Chem. B 104 (2000) 12119–12129.
[41] H.I. Petrache, A. Salmon, M.F. Brown, Structural properties of docosahexaenoyl phospholipid bilayers investigated by solid-state ^{2}H NMR spectroscopy, J. Am. Chem. Soc. 123 (2001) 12611–12622.
[42] A.A. Nevzorov, S. Moltke, M.P. Heyn, M.F. Brown, Solid-state NMR line shapes of uniaxially oriented immobile systems, J. Am. Chem. Soc. 121 (1999) 7636–7643.
[43] J. Saam, E. Tajkhorshid, S. Hayashi, K. Schulten, Molecular dynamics investigation of primary photoinduced events in the activation of rhodopsin, Biophys. J. 83 (2002) 3097–3112.
[44] P.S. Crozier, M.J. Stevens, L.R. Forrest, T.B. Woolf, Molecular dynamics simulation of dark-adapted rhodopsin in an explicit membrane bilayer: coupling between local retinal and larger scale conformational change, J. Mol. Biol. 333 (2003) 493–514.
[45] A. Grossfield, S.E. Feller, M.C. Pitman, Contribution of omega-3 fatty acids to the thermodynamics of membrane protein solvation, J. Phys. Chem. B 110 (2006) 8907–8909.
[46] A. Grossfield, S.E. Feller, M.C. Pitman, A role for direct interactions in the modulation of rhodopsin by ω-3 polyunsaturated lipids, Proc. Natl. Acad. Sci. U.S.A. 103 (2006) 4888–4893.
[47] X. Periole, T. Huber, S.J. Marrink, T.P. Sakmar, G protein-coupled receptors self-assemble in dynamics simulations of model bilayers, J. Am. Chem. Soc. 129 (2007) 10126–10132.
[48] M. Neri, S. Vanni, I. Tavernelli, U. Rothlisberger, Role of aggregation in rhodopsin signal transduction, Biochemistry 49 (2010) 4827–4832.
[49] G. Khelashvili, A. Grossfield, S.E. Feller, M.C. Pitman, H. Weinstein, Structural and dynamic effects of cholesterol at preferred sites of interaction with rhodopsin identified from microsecond length molecular dynamics simulations, Proteins 76 (2009) 403–417.
[50] G. Khelashvili, S. Mondal, O.S. Andersen, H. Weinstein, Cholesterol modulates the membrane effects and spatial organization of membrane-penetrating ligands for G-protein coupled receptors, J. Phys. Chem. B 114 (2010) 12046–12057.
[51] E.C.Y. Yan, M.A. Kazmi, Z. Ganim, J.-M. Hou, D. Pan, B.S.W. Chang, T.P. Sakmar, R.A. Mathies, Retinal counterion switch in the photoactivation of the G protein-coupled receptor rhodopsin, Proc. Natl. Acad. Sci. U.S.A. 100 (2003) 9262–9267.
[52] S. Lüdeke, R. Beck, E.C.Y. Yan, T.P. Sakmar, F. Siebert, R. Vogel, The role of Glu181 in the photoactivation of rhodopsin, J. Mol. Biol. 353 (2005) 345–356.
[53] U.F. Röhrig, L. Guidoni, U. Rothlisberger, Early steps of the intramolecular signal transduction in rhodopsin explored by molecular dynamics simulations, Biochemistry 41 (2002) 10799–10809.
[54] U.F. Röhrig, D. Sebastiani, NMR chemical shifts of the rhodopsin chromophore in the dark state and in bathorhodopsin: a hybrid QM/MM molecular dynamics study, J. Phys. Chem. B 112 (2008) 1267–1274.
[55] K. Martínez-Mayorga, M.C. Pitman, A. Grossfield, S.E. Feller, M.F. Brown, Retinal counterion switch mechanism in vision evaluated by molecular simulations, J. Am. Chem. Soc. 128 (2006) 16502–16503.
[56] J. Li, P.C. Edwards, M. Burghammer, C. Villa, G.F.X. Schertler, Structure of bovine rhodopsin in a trigonal crystal form, J. Mol. Biol. 343 (2004) 1409–1438.
[57] K. Henzler-Wildman, D. Kern, Dynamic personalities of proteins, Nature 450 (2007) 964–972.
[58] N.J. Gibson, M.F. Brown, Membrane lipid influences on the energetics of the metarhodopsin I and metarhodopsin II conformational states of rhodopsin probed by flash photolysis, Photochem. Photobiol. 54 (1991) 985–992.
[59] M.F. Brown, Modulation of rhodopsin function by properties of the membrane bilayer, Chem. Phys. Lipids 73 (1994) 159–180.

[60] Y. Wang, A.V. Botelho, G.V. Martinez, M.F. Brown, Electrostatic properties of membrane lipids coupled to metarhodopsin II formation in visual transduction, J. Am. Chem. Soc. 124 (2002) 7690–7701.
[61] A.V. Botelho, T. Huber, T.P. Sakmar, M.F. Brown, Curvature and hydrophobic forces drive oligomerization and modulate activity of rhodopsin in membranes, Biophys. J. 91 (2006) 4464–4477.
[62] P.-W. Lau, A. Grossfield, S.E. Feller, M.C. Pitman, M.F. Brown, Dynamic structure of retinylidene ligand of rhodopsin probed by molecular simulations, J. Mol. Biol. 372 (2007) 906–917.
[63] R. Vogel, F. Siebert, S. Lüdeke, A. Hirshfeld, M. Sheves, Agonists and partial agonists of rhodopsin: retinals with ring modifications, Biochemistry 44 (2005) 11684–11699.
[64] A.B. Patel, E. Crocker, M. Eilers, A. Hirshfeld, M. Sheves, S.O. Smith, Coupling of retinal isomerization to the activation of rhodopsin, Proc. Natl. Acad. Sci. U.S.A. 101 (2004) 10048–10053.
[65] P.J.R. Spooner, J.M. Sharples, S.C. Goodall, P.H.M. Bovee-Geurts, M.A. Verhoeven, J. Lugtenburg, A.M.A. Pistorius, W.J. DeGrip, A. Watts, The ring of the rhodopsin chromophore in a hydrophobic activation switch within the binding pocket, J. Mol. Biol. 343 (2004) 719–730.
[66] M.F. Brown, Theory of spin–lattice relaxation in lipid bilayers and biological membranes. ^{2}H and ^{14}N quadrupolar relaxation, J. Chem. Phys. 77 (1982) 1576–1599.
[67] D.A. Torchia, A. Szabo, Spin–lattice relaxation in solids, J. Magn. Reson. 49 (1982) 107–121.
[68] T. Huber, A.V. Botelho, K. Beyer, M.F. Brown, Membrane model for the GPCR prototype rhodopsin: hydrophobic interface and dynamical structure, Biophys. J. 86 (2004) 2078–2100.
[69] S. Hayashi, E. Tajkhorshid, K. Schulten, Photochemical reaction dynamics of the primary event of vision studied by means of a hybrid molecular simulation, Biophys. J. 96 (2009) 403–416.
[70] R. Vogel, S. Lüdeke, F. Siebert, T.P. Sakmar, A. Hirshfeld, M. Sheves, Agonists and partial agonists of rhodopsin: retinal polyene methylation affects receptor activation, Biochemistry 45 (2006) 1640–1652.
[71] S.E. Feller, K. Gawrisch, T.B. Woolf, Rhodopsin exhibits a preference for solvation by polyunsaturated docosohexaenoic acid, J. Am. Chem. Soc. 125 (2003) 4434–4435.
[72] B. Mertz, M. Lu, M.F. Brown, S.E. Feller, Steric and electronic influences on the torsional energy landscape of retinal, Biophys. J. 101 (2011) L17–L19.
[73] P.J.R. Spooner, J.M. Sharples, M.A. Verhoeven, J. Lugtenberg, C. Glaubitz, A. Watts, Relative orientation between the β-ionone ring and the polyene chain for the chromophore of rhodopsin in native membranes, Biochemistry 41 (2002) 7549–7555.
[74] P.J.R. Spooner, J.M. Sharples, S.C. Goodall, H. Seedorf, M.A. Verhoeven, J. Lugtenburg, P.H.M. Bovee-Geurts, W.J. DeGrip, A. Watts, Conformational similarities in the β-ionone ring region of the rhodopsin chromophore in its ground state and after photoactivation to the metarhodopsin-I intermediate, Biochemistry 42 (2003) 13371–13378.
[75] B. Knierim, K.P. Hofmann, O.P. Ernst, W.L. Hubbell, Sequence of late molecular events in the activation of rhodopsin, Proc. Natl. Acad. Sci. U.S.A. 104 (2007) 20290–20295.
[76] R. Vogel, M. Mahalingam, S. Lüdeke, T. Huber, F. Siebert, T.P. Sakmar, Functional role of the "ionic lock"—an interhelical hydrogen-bond network in family A heptahelical receptors, J. Mol. Biol. 380 (2008) 648–655.
[77] S. Arnis, K.P. Hofmann, Two different forms of metarhodopsin II: Schiff base deprotonation precedes proton uptake and signaling state, Proc. Natl. Acad. Sci. U.S.A. 90 (1993) 7849–7853.
[78] M. Mahalingam, K. Martínez-Mayorga, M.F. Brown, R. Vogel, Two protonation switches control rhodopsin activation in membranes, Proc. Natl. Acad. Sci. U.S.A. 105 (2008) 17795–17800.